Temperature dependent frequency tuning of NbO_X relaxation oscillators

Sanjoy Kumar Nandi, Shuai Li, Xinjun Liu, and Robert G. Elliman

Citation: Appl. Phys. Lett. **111**, 202901 (2017); doi: 10.1063/1.4999373
View online: https://doi.org/10.1063/1.4999373
View Table of Contents: http://aip.scitation.org/toc/apl/111/20
Published by the American Institute of Physics

Temperature dependent frequency tuning of NbO_x relaxation oscillators

Sanjoy Kumar Nandi,[1,a),b)] Shuai Li,[1,a)] Xinjun Liu,[1,2,c)] and Robert G. Elliman[1]
[1]*Department of Electronic Materials Engineering, Research School of Physics and Engineering, The Australian National University, Canberra ACT 2601, Australia*
[2]*Tianjin Key Laboratory of Low Dimensional Materials Physics and Preparation Technology, Faculty of Science, Tianjin University, Tianjin 300354, China*

(Received 7 August 2017; accepted 30 October 2017; published online 14 November 2017)

This study investigates the temperature dependence of current-controlled negative differential resistance (CC-NDR) in Pt/NbO_x/TiN devices and its effect on the dynamics of associated Pearson-Anson relaxation oscillators. The voltage range over which CC-NDR is observed decreases with increasing temperature such that no NDR is observed for temperatures above ~380 K. Up to this temperature, relaxation oscillators exhibit voltage and temperature dependent oscillation frequencies in the range of 1 to 13 MHz. Significantly, the sensitivity of the frequency to temperature changes was found to be voltage-dependent, ranging from 39.6 kHz/K at a source voltage of 2 V to 110 kHz/K at a source voltage of 3 V, in the temperature range of 296–328 K. Such a behaviour provides insights into temperature tolerance and tuning variability for environmentally sensitive neuromorphic computing. *Published by AIP Publishing.*
https://doi.org/10.1063/1.4999373

Threshold switching in thin-film transition-metal-oxides (e.g., VO_x, NbO_x, and TiO_x) is of interest for neuromorphic computing.[1] This derives from the fact that simple two terminal devices (metal-insulator-metal) exhibit current controlled negative differential resistance (CC-NDR) and can be used to fabricate a voltage controlled relaxation oscillator.[1,2] When appropriately coupled, such oscillators exhibit complex nonlinear dynamics, including many of the characteristics of biological neurons, such as threshold spiking and voltage dependent frequency modulation. To fully exploit the capabilities of these devices, it is necessary to understand their limitations and dependencies.

Among the materials investigated, vanadium dioxide (VO_2) is the most well studied and exploited. However, the CC-NDR in this material results from a Mott-Peierls transition at a temperature of 340 K.[3–6] This precludes its use in many microelectronics applications, where the expectation is that devices will operate at temperatures approaching 400 K. To address this limitation, recent interest has been focused on NbO_x which has demonstrated higher operating temperatures.[7,9] The threshold switching mechanism in NbO_x is still under debate.[8–12]

The temperature dependence of threshold switching (CC-NDR) has been studied in VO_2,[13] Ti_4O_7,[14] Ta_2O_5,[15] and NbO_2[7,9] systems. However, the temperature dependence of self-oscillation in these transition-metal-oxides has received far less attention. Kim *et al.*[16] showed that the oscillation frequency of planar VO_2 two terminal devices increased with increasing temperature but provided little insight into the effect of temperature on frequency tuning (increase in frequency with applied voltage) or the frequency range. In this study, we report on the temperature dependence of CC-NDR in Pt/NbO_x/TiN devices and its effect on the dynamics of a Pearson-Anson relaxation oscillator based on these devices.

Test devices consisted of Pt/NbO_x/TiN capacitor structures, fabricated on oxidized (100) silicon wafers by successive layer deposition, as depicted in Fig. 1(a). First, a 50 nm thick layer of TiN was sputtered onto the wafer to form the bottom electrode. This was followed by a ~50 nm thick layer of the NbO_x layer deposited by dc reactive-sputter deposition using an Nb target and an O_2/Ar ambient. Finally, a 50 nm thick Pt layer was deposited through a shadow mask by electron beam evaporation to define top contact pads with diameters in the range of 100–200 μm.

The stoichiometry of the NbO_x film was confirmed to be near Nb_2O_5 (i.e., $x = 2.5$) by He^+-ion Rutherford back scattering spectrometry,[17] and the amorphous nature of the film was confirmed by electron diffraction patterns. The layer thicknesses and structure were further confirmed by transmission electron microscopy (TEM) of sample cross-sections, as shown in Fig. 1(b).

Electrical characterization was performed using an Agilent B1500A semiconductor parametric analyzer attached to a Signatone probestation with a heating stage. DC current-voltage (I–V) characteristics were determined by direct probing of the top and bottom electrodes, and oscillation characteristics were studied by adding a series resistor between the voltage source and the top contact to form a simple Pearson-Anson oscillator circuit, as shown in Fig. 2(a).

To initiate oscillation, a voltage pulse of 3 μs duration was applied to the load resistor attached to the top electrode of the device. Device current oscillations were measured by employing a Tektronix TPS2024B digital oscilloscope to monitor the voltage drop across the 50 Ω monitor resistor. Temperature dependent measurements were performed in air. Some comparative studies were also performed on the Pt/Nb_2O_5/Nb device structure (see supplementary material), the details of which have been reported in our previous

[a)]S. K. Nandi and S. Li contributed equally to this work.
[b)]Email: sanjoy.nandi@anu.edu.au
[c)]Email: xinjun.liu@tju.edu.cn

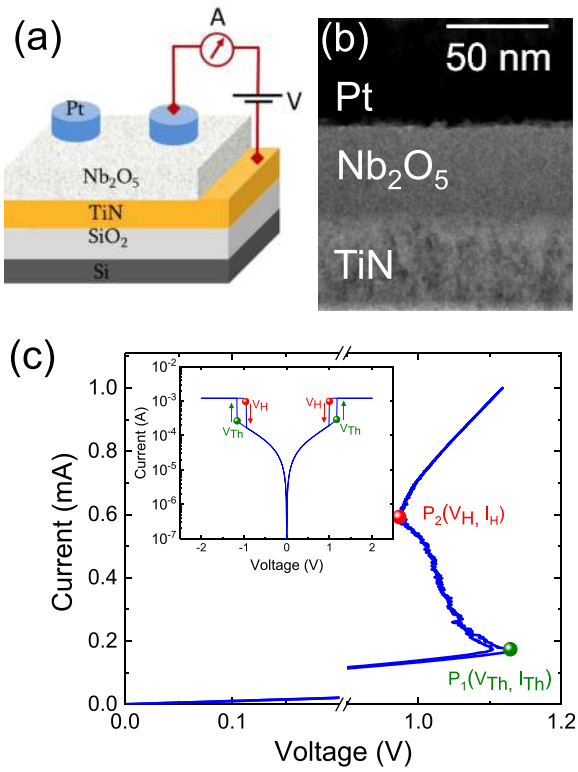

FIG. 1. (a) Schematic of the device structure, (b) a TEM image of a sample cross-section, confirming the Pt/NbO_x/TiN device structure and (c) measured I–V characteristics during current-controlled sweeps showing clear NDR characteristics (the inset shows the symmetric voltage controlled threshold switching). The NDR region forms the basis of the relaxation oscillator.

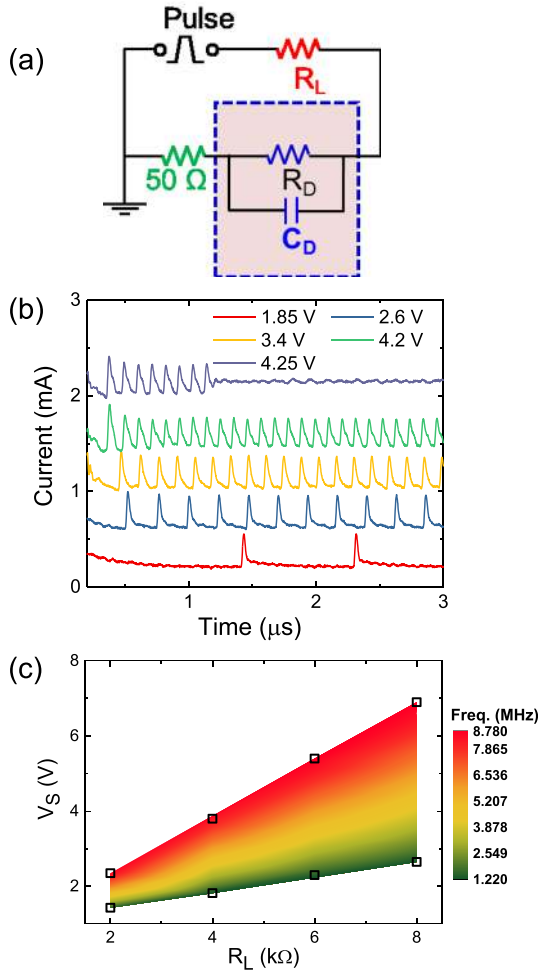

FIG. 2. (a) Schematic of the electrical circuit used to observe dynamics of self-oscillations, where R_D and C_D represent the device resistance and capacitance, respectively. (b) Measured oscillation waveform of the device current (I_{Device}) in the 50 Ω resistor for 3 μs source voltage (V_S) pulses in the range of 1.85 to 4.25 V and a series resistor of 4 kΩ. (c) Oscillation window defined by V_S and R_L with oscillation frequency depicted by shading. The black squares are from load line analysis.

studies.[18,19] Note that I–V characteristics were measured with negative bias applied to the top electrode unless otherwise stated.

The as-fabricated devices were in a high resistance state and required an electroforming step to initiate a threshold-switching response. This was achieved by applying a negative bias to the top Pt electrode and sweeping the bias voltage until a rapid increase in current was observed, using a compliance limit of 4 mA. This typically required voltages of ∼−10 V and resulted in a permanent reduction in the low-voltage resistance of the device. Symmetric threshold switching was observed immediately following the electroforming process, and after several switching cycles, the characteristics were stable and reproducible, as shown the inset in Fig. 1(c). There is some evidence that an active interlayer forms at the reactive-metal/oxide interface during the initial cycling and that this plays an important role in the switching response.[20–22]

Figure 1(c) shows a current-controlled I–V sweep for the device after stabilization. The region of CC-NDR is bound by the threshold point P_1 (V_{Th}, I_{Th}) and the hold point P_2 (V_H, I_H) and corresponds to a region in which the conductivity of the sample increases rapidly. For currents above the hold-current, I_H, the conductivity reaches a maximum and the device exhibits near-Ohmic behaviour. The device therefore exhibits three distinct regimes as the current increases, a pre-threshold regime, a negative differential regime, and a saturation regime. For a device voltage of 1.05 V, the effective resistances in these regimes are 3.8 kΩ, −436 Ω, and +407 Ω, respectively. The NDR response in NbO_x is believed to result from local Joule heating and an associated change in conductivity due to Poole-Frenkel (P-F) conduction,[10] a Mott insulator-metal transition (IMT),[23] or other mechanisms. As noted in the introduction, there is growing consensus that P-F conduction can account for the NDR, but there is also evidence that the process is more complicated. For example, recent studies have demonstrated the existence of two distinct NDR regions under high-current operation, one attributed to P-F conduction and the other to a Mott IMT.[12] These observations suggest that further work is required to fully understand the NDR response, but this is beyond the scope of the present study.

Oscillator dynamics were studied using the Pearson-Anson oscillator circuit shown schematically in Fig. 2(a) and discussed previously for similar devices.[19] The conditions for stable oscillation were determined from load line analysis,[2] and Fig. 2(b) illustrates typical behavior as a function of source voltages for a constant load resistance of 4.0 kΩ. The corresponding V_S-R_L oscillation window and frequency are shown in Fig. 2(c) for room temperature operation.[24] From

load line analysis, it is found that the voltage window for stable oscillation ranges from $V_{S,min}$ to $V_{S,max}$, where $V_{S,min} = V_{th} + (R_L + 50)\, I_{th}$ and $V_{S,max} = V_h + (R_L + 50)\, I_h$. For a given load resistance, the oscillation frequency is observed to increase from around 1.2 to 8.8 MHz as the voltage is varied from $V_{S,min}$ to $V_{S,max}$. Since the voltage window increases with increasing load resistance, the voltage-tuning sensitivity decreases from 7.57 MHz/V for R_L equal to 2 kΩ to 1.77 MHz/V for R_L equal to 8 kΩ.

Oscillations are maintained by the device switching between high and low resistance states; switching from high-to-low resistance effectively shorts the device and causes a sudden reduction (increase) in device voltage (current), with the load resistor acting as a voltage divider. The RC time constant of the circuit is reduced due to the lower device resistance, and the device voltage (current) decreases (increases) rapidly. As the voltage drops below its hold value, the device switches back to its high resistance state and the voltage (current) increases (decreases) with the longer RC time constant associated with the higher device resistance. When the voltage again exceeds the threshold value, the device switches back to its low resistance state and the process repeats. The asymmetric current-waveforms shown in Fig. 2(b) reflect the different RC time-constants associated with the high-to-low and low-to-high transitions, as well as contributions from parasitic and device capacitances. These contributions have been discussed in detail in Ref. 24.

Figure 3 shows measured I–V characteristics [Fig. 3(a)] and corresponding threshold- and hold-voltages and currents [Fig. 3(b)] as a function of device temperature. Both the threshold and the hold voltages decrease with increasing temperature, as does the difference between them. As a consequence, the CC-NDR region decreases with increasing temperature and is effectively eliminated for temperatures above ~378 K.

The effect of these changes on the oscillation behaviour was studied using the circuit in Fig. 2(a) with a load resistance of 4 kΩ. The choice of load resistance is largely arbitrary as it is temperature independent, but it does determine the voltage range over which oscillations are observed, as shown in Fig. 2(c). Figure 4(a) shows the oscillator response as a function of temperature for an applied bias of 2.4 V. This shows that the oscillation frequency increases and that the oscillation amplitude decreases with increasing temperature. The reduction in amplitude is consistent with the observed reduction in the threshold- and hold-voltages, and the oscillation window can be determined from the CC-NDR curves shown in Fig. 3(a) using load line analysis. In this figure, the points indicate the window-boundaries determined from load-line analysis, and the color-coded data define the region in which oscillations were directly measured.

The effect of temperature on the oscillation frequency is shown color-coded in Fig. 4(b) and explicitly in Fig. 4(c). For a fixed source voltage and load resistance, the frequency is observed to increase with increasing temperature, as expected from the change in the CC-NDR characteristics. For example, by assuming that the oscillation frequency is limited by the slower time constant of the low-to-high transition and that the monitor resistor can be ignored, the low-frequency behavior has the following form:[25]

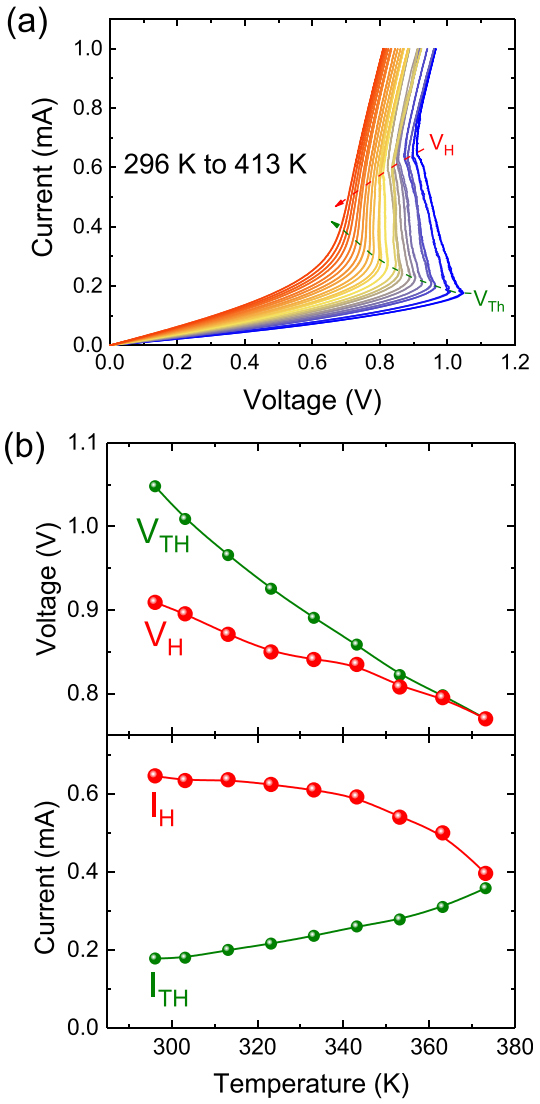

FIG. 3. (a) CC-NDR as a function of temperature; (b) absolute values of the hold and threshold points (voltage and current) as a function of temperature.

$$f = \left[R' C_D \ln \frac{(\alpha V_s - V_H)}{(\alpha V_s - V_{Th})} \right]^{-1}, \tag{1}$$

where $R' = R_D R_L/(R_D + R_L)$ and $\alpha = R_D/(R_D + R_L)$. Since V_{Th} decreases more rapidly with temperature than V_H, as shown in Fig. 3(b), the frequency is predicted to increase with temperature. However, this simple analysis ignores the temperature dependence of device resistance (R_D) and capacitance (C_D) and therefore overestimates the temperature sensitivity and does not account for the dynamics of the resistive and capacitive device currents, as previously discussed.[24]

The data in Fig. 4 highlight the important functionality of these relaxation oscillators, including the temperature dependent oscillation frequency, the ability to program the oscillator frequency, and its temperature coefficient using the source voltage. The latter is evident from the data in Fig. 4(c), which shows an increasing frequency span as the voltage increases. For example, in the temperature range of 296 – 328 K, the temperature coefficient ranges from 39.6 kHz/K at a source voltage of 2 V to 110 kHz/K at a source voltage of 3 V.

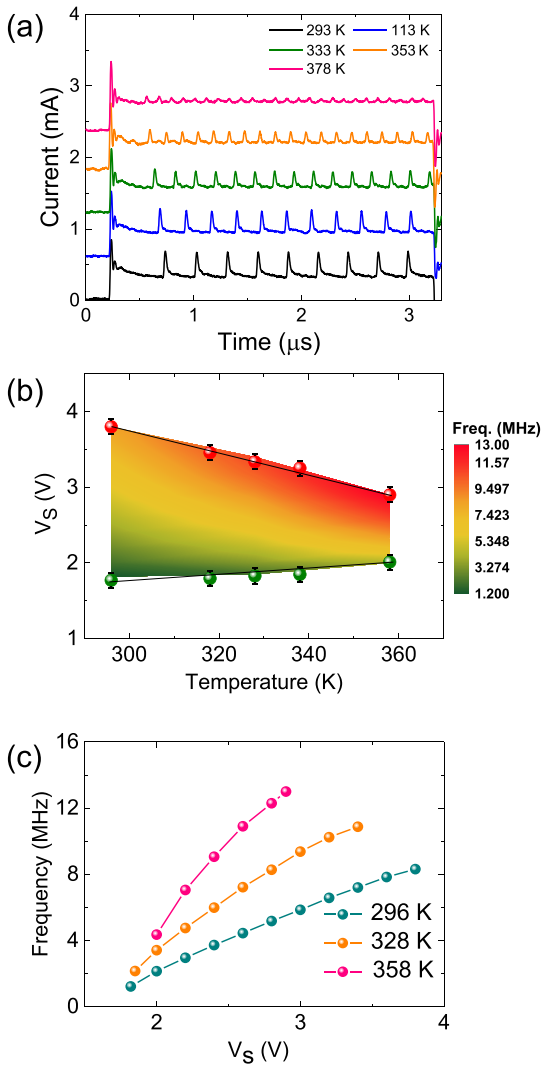

FIG. 4. (a) Oscillation as a function of temperature for an applied pulse of 2.4 V and 3 μs and (b) measured oscillation window as a function of temperature with a constant load resistor of 4 kΩ. The oscillation frequency depicted by colour shading, and the green/red circles are from load line analysis for corresponding temperature. (c) Frequency as a function of applied bias at three different temperatures.

In summary, we have reported the temperature dependence of the CC-NDR response in Pt/NbO_x/TiN devices and its effect on the dynamics of a Pearson-Anson relaxation oscillator. These results highlight the voltage and temperature tunability of CC-NDR based relaxation oscillations and provide the basis for devices with temperature dependent functionality for environmentally sensitive neuromorphic computing.

See supplementary material for oscillation properties of the Pt/Nb_2O_5/Nb device structure.

This work was supported by the Australian Research Council and relied on access to facilities funded under the Australian Government's NCRIS program. We want to acknowledge the Australian National Fabrication Facility (ANFF) ACT node in carrying out this research. The authors also acknowledge the facilities and the scientific and technical assistance of the Australian Microscopy & Microanalysis Research Facility at the Centre of Advanced Microscopy, The Australian National University, and Professor Dougal G. McCulloch, RMIT University, for TEM analysis [Figure S1(a)].

[1]M. D. Pickett, G. Medeiros-Ribeiro, and R. S. Williams, Nat. Mater. **12**(2), 114 (2013).
[2]N. Shukla, A. Parihar, E. Freeman, H. Paik, G. Stone, V. Narayanan, H. Wen, Z. Cai, V. Gopalan, and R. Engel-Herbert, Sci. Rep. **4**, 4964 (2014).
[3]S. Kumar, M. D. Pickett, J. P. Strachan, G. Gibson, Y. Nishi, and R. S. Williams, Adv. Mater. **25**(42), 6128–6132 (2013).
[4]S. Rathi, J.-H. Park, I.-Y. Lee, J. M. Baik, K. S. Yi, and G.-H. Kim, J. Phys. D: Appl. Phys. **47**(29), 295101 (2014).
[5]A. Gentle and G. Smith, J. Phys. D: Appl. Phys. **41**(1), 015402 (2008).
[6]S. Kittiwatanakul, S. A. Wolf, and J. Lu, Appl. Phys. Lett. **105**(7), 073112 (2014).
[7]Y. Wang, R. B. Comes, S. A. Wolf, and J. Lu, IEEE J. Electron Devices Soc. **4**(1), 11–14 (2016).
[8]A. O'Hara, T. N. Nunley, A. B. Posadas, S. Zollner, and A. A. Demkov, J. Appl. Phys. **116**(21), 213705 (2014).
[9]S. Li, X. Liu, S. Nandi, D. Venkatachalam, and R. Elliman, in *Proceedings of 2014 Conference on Optoelectronic and Microelectronic Materials Devices (COMMAD), Perth, Australia, 14–17 December 2014* (IEEE, 2014), pp. 138–140.
[10]S. Slesazeck, H. Mähne, H. Wylezich, A. Wachowiak, J. Radhakrishnan, A. Ascoli, R. Tetzlaff, and T. Mikolajick, RSC Adv. **5**(124), 102318–102322 (2015).
[11]B. Wu, A. Zimmers, H. Aubin, R. Ghosh, Y. Liu, and R. Lopez, Phys. Rev. B **84**(24), 241410 (2011).
[12]S. Kumar, Z. Wang, N. Davila, N. Kumari, K. J. Norris, X. Huang, J. P. Strachan, D. Vine, A. D. Kilcoyne, and Y. Nishi, Nat. Commun. **8**, 658 (2017).
[13]A. Pergament, P. Boriskov, A. Velichko, and N. Kuldin, J. Phys. Chem. Solids **71**(6), 874–879 (2010).
[14]M. D. Pickett, J. Borghetti, J. J. Yang, G. Medeiros-Ribeiro, and R. S. Williams, Adv. Mater. **23**(15), 1730–1733 (2011).
[15]A. A. Sharma, Y. Li, M. Skowronski, J. A. Bain, and J. A. Weldon, IEEE Trans. Electron Devices **62**(11), 3857–3862 (2015).
[16]B.-J. Kim, G. Seo, Y. W. Lee, S. Choi, and H.-T. Kim, IEEE Electron Device Lett. **31**(11), 1314–1316 (2010).
[17]M. Vos, X. Liu, P. L. Grande, S. K. Nandi, D. K. Venkatachalam, and R. G. Elliman, Nucl. Instrum. Methods Phys. Res. Sect. B **340**(0), 58–62 (2014).
[18]S. Li, X. Liu, S. K. Nandi, D. K. Venkatachalam, and R. G. Elliman, Nanotechnology **28**(12), 125201 (2017).
[19]S. Li, X. Liu, S. K. Nandi, D. K. Venkatachalam, and R. G. Elliman, Appl. Phys. Lett. **106**(21), 212902 (2015).
[20]S. K. Nandi, X. Liu, D. K. Venkatachalam, and R. G. Elliman, J. Phys. D: Appl. Phys. **48**(19), 195105 (2015).
[21]X. Liu, S. K. Nandi, D. K. Venkatachalam, K. Belay, S. Song, and R. G. Elliman, IEEE Electron Device Lett. **35**(10), 1055–1057 (2014).
[22]D.-Y. Cho, M. Luebben, S. Wiefels, K.-S. Lee, and I. Valov, ACS Appl. Mater. Interfaces **9**(22), 19287–19295 (2017).
[23]M. D. Pickett and R. S. Williams, Nanotechnology **23**(21), 215202 (2012).
[24]X. Liu, S. Li, S. K. Nandi, D. K. Venkatachalam, and R. G. Elliman, J. Appl. Phys. **120**(12), 124102 (2016).
[25]P. E. Schmidt and R. C. Callarotti, J. Appl. Phys. **55**(8), 3144–3147 (1984).